



## Journal of Advanced Research in Fluid Mechanics and Thermal Sciences

Journal homepage:  
[https://semarakilmu.com.my/journals/index.php/fluid\\_mechanics\\_thermal\\_sciences/index](https://semarakilmu.com.my/journals/index.php/fluid_mechanics_thermal_sciences/index)  
ISSN: 2289-7879



# Influence of the Aspect Ratio on the Free Convection Heat Transmission Properties of a Container Containing Porous Materials

Alaa Hadi Darweesh<sup>1,\*</sup>, Zena Khalefa Kadhim<sup>1</sup>

<sup>1</sup> Department of Mechanical Engineering, College of Engineering, Wasit University, Kut, Iraq

ARTICLE INFO	ABSTRACT
<p><b>Article history:</b> Received 13 April 2022 Received in revised form 27 July 2022 Accepted 10 August 2022 Available online 6 September 2022</p> <p><b>Keywords:</b> Natural convection; experimental study; porous media; modified Rayleigh number; Nusselt number</p>	<p>Nowadays, many industrial and modern applications depend on heat transport in porous zones. An experimental study of the natural convection heat transfer in a corrugated cavity with dimensions of (200, 250, 300) mm in length, a width of 200 mm, a depth of 27 mm, and an amplitude of 30 mm was filled with porous materials: glass balls (3, 6, 10) mm and alumina balls (6) mm, where the water was the working fluid. The top surface was exposed to the environment, while the bottom surface was subjected to constant heat flux (300, 500, 700, 900, 1100 W/m<sup>2</sup>), The front face, back face, and sides were insulated. In this study, temperature distribution, modified Rayleigh number, and Nusselt number values are foremost criteria, which are presented for three levels of aspect ratio. The influence of various aspect ratios on heat transfer is investigated. The results showed that the heat transfer coefficient decreases with the increase in aspect ratio. The highest value is when aspect ratio = 1. The enhanced Rayleigh number decreases as the aspect ratio increases by 10%.</p>

## 1. Introduction

The studies of enhancement convective heat transfer inside the cavities have received the attention of many researchers to study the parameters that effect on heat transfer because of its multiple engineering applications such as nuclear and solar collectors, electronic equipment cooling and tubular heat exchanger, Steel suspension cables, oil well drilling and rotating shafts investigated by Nield and Bejan [1].

An inclined rectangular enclosure with a sinusoidal temperature profile on the left wall was employed, whereas a computational analysis of the heat transfer and free convection flow was carried out by Cheong *et al.*, [2]. The enclosure's top and bottom walls were maintained as adiabatic. For all aspect ratios and Rayleigh numbers, the heat transmission was first increased and then dropped as the enclosure inclination became bigger. For all considered Rayleigh numbers, increasing the aspect ratio yield a declining trend in heat transmission. Gati'a *et al.*, [3] performed an experimental and numerical examination regarding the laminar free convection heat issue. By using

\* Corresponding author.

E-mail address: [alaa301@uowasit.edu.iq](mailto:alaa301@uowasit.edu.iq)

<https://doi.org/10.37934/arfmts.99.1.174195>

water, a saturated silica-sand porous combination was studied. Various variables were examined, including the phase angle, the aspect ratio, and the waving of the container sidewalls in a sinusoidal form. Unless the number of the waves per cavity height equals one, the results show that the cavity's walls have a sinusoidal curviness that leads to a reduction in the heat transfer rate (i.e.,  $N = 1$ ). When the wave's amplitude is almost comparable to one, the heat transfer rate within the cavity is enhanced (amplitude = 0.075). Mehryan *et al.*, [4] investigated the  $\text{Al}_2\text{O}_3$ -Cu water hybrid nanofluid's free convective heat transport properties in a cavity filled with a porous material. Glass balls and aluminum metal foam are considered two significant types of porous media that are taken into account for the porous matrix. From these findings, it was demonstrated that the utilization of nanoparticles in porous material could lead to a reduction in heat transport. When compared to a single nanofluid, the observed reduction in the heat transfer rate was substantially larger for hybrid nanofluids. Ali *et al.*, [5] carried out a numerical analysis in rectangular cavity. The bottom and top walls are subjected to constant high temperature ( $T_h$ ) and low temperature ( $T_c$ ) respectively. The side walls are treated as adiabatic. The top wall moves in the positive x-direction. the hybrid nanofluid ( $\text{Al}_2\text{O}_3$ -Cu-water) is used to enhance the heat transfer. The Finite-Volume-Method (FVM) along with the SIMPLE-algorithm has been utilized to study the heat-transfer and, mixed convection fluid-flow of the hybrid nanofluid ( $\text{Al}_2\text{O}_3$ -Cu-water). The effects of Reynolds number and hybrid nanoparticle volume fraction on the flow field have been investigated. It is found that the mean Nusselt number increases with respect to Reynolds numbers and hybrid nano- particle volume fraction. A numerical investigation of conjugate natural convection inside a divided square cavity filled with  $\text{Al}_2\text{O}_3$ -water nanofluid is performed by Ferhi *et al.*, [6]. The lattice Boltzmann method (LBM) is used to solve the governing equations. The study of the conjugate heat transfer and nonliquid motion is, afterward, conducted for the ranges of nanoparticles volume fraction (%):  $1 \leq \phi \leq 4$ , temperature ( $^\circ\text{C}$ ):  $20 \leq T \leq 40$ , particle size (nm):  $15 \leq dp \leq 120$  and Rayleigh number:  $103 \leq Ra \leq 106$ . Results show a heat transfer rise by increasing the temperature. However, for the  $\text{Al}_2\text{O}_3$  nanoparticles size, the enhancement marked a maximum close to  $dp=33\text{nm}$  in a concave behavior. The heat transfer and the fluid motion are dumped by increasing the volume fraction  $\phi$  (%) and the nanoparticles size ( $dp \geq 35\text{nm}$ ) due to the reduced effective  $Ra^*$  number. Mahdavi *et al.*, [7] conducted numerical studies and experimental evaluations of the hydrodynamics and heat transfer properties of water flow through a pipe with the insertion of a porous material at the core. The heat flux that was applied to the pipe wall was consistent and homogenous. The copper wires that made up the porous cylinder were also weaved together. The outcomes were evaluated against the case without a porous insert. The outcomes also demonstrated that the impact of the inertial coefficient and the thermal conductivity ratio become more pronounced as the thickness of the porous media was increased. However, especially for porous inserts with radii near pipe radii, the impact of the Prandtl number was less substantial. Cimpean *et al.*, [8] analyzed the free convection in an inclined square cavity filled with a fluid-saturated porous medium with sinusoidal temperature distribution on the side walls. The parameters related to the sinusoidal temperature at the walls and to the inclination angle of the cavity affect the convective pattern and transport flux such that the change in the phase deviation of the sinusoidal temperature leads to a significant change in the convective cells of the cavity. Also, by inclining the cavity, the behavior of the convective cells is completely changed comparing to no inclination of it. Bakar *et al.*, [9] study numerically the effect of internal heat generation or absorption in a two-dimensional (2D) horizontal cavity to the fluid flow and heat transfer process. The vertical walls are well insulated. Meanwhile, the top and bottom walls are kept at  $T_h$  and  $T_c$ , respectively, where  $T_h > T_c$ . The top wall moves at a constant speed from left to right.  $T$ . It is found that the presence of heat generation or absorption has a significant effect on the fluid flow and heat transfer process in the horizontal cavity. Overall, for internal heat generation, the heat transfer rate decreases, while the

opposite pattern can be observed for the case of internal heat absorption. However, for  $Ri = 10.0$ , as the heat generation's value increases from 2 to 4, the heat transfer rate is the same. Barman and Rao [10] study numerically the effect of aspect ratio on natural convection in a wavy porous cavity. The cavity is placed vertically, and its right wavy wall is kept at fixed low temperature, whereas a partial heat source is embedded at the left vertical wall keeping top and bottom walls as adiabatic. The non-dimensional governing equations describing Darcy flow are solved by the finite difference method. The parameters involving the investigation are aspect ratio ( $As = 0.2, 0.5, 2.0, 5.0$ ), Rayleigh-Darcy number ( $Ra = 10, 10^2, 10^3$ ). The increment in aspect ratio increases the cooling efficiency of the heat source. Al-Farhany and Abdulsahib [11] did a numerical study of mixed convective heat transfer in a square enclosure partitioned in two layers with a rotating circular cylinder at the middle of the cavity. The experiments are performed with  $Al_2O_3$ -water nanofluid (upper layer) and superposed porous medium (lower layer). The upper and lower horizontal walls are assumed to be insulated, while the left and right walls are kept at high and low temperature respectively. This study is focused to investigate the effect of Darcy number ( $10^{-2} \leq Da \leq 10^{-5}$ ), Rayleigh number ( $10^3 \leq Ra \leq 10^6$ ) on the heat transfer and fluid flow. The results show that the intensity of the flow, steep temperature gradient, and the average Nusselt number ( $Nu$ ) increase with increasing the value of Darcy number, Rayleigh number.

In previous years, although the application of porous materials to improve heat transfer has been widely reported in the literature, the majority of the related works are theoretical. Therefore, in this work, an experimental study was conducted to study the influence of the aspect ratio on the natural convection characteristics in a cavity filled with glass and alumina balls with saturated water.

## 2. Experimental Apparatus

The test rig, shown in Figure 1, includes the following components.

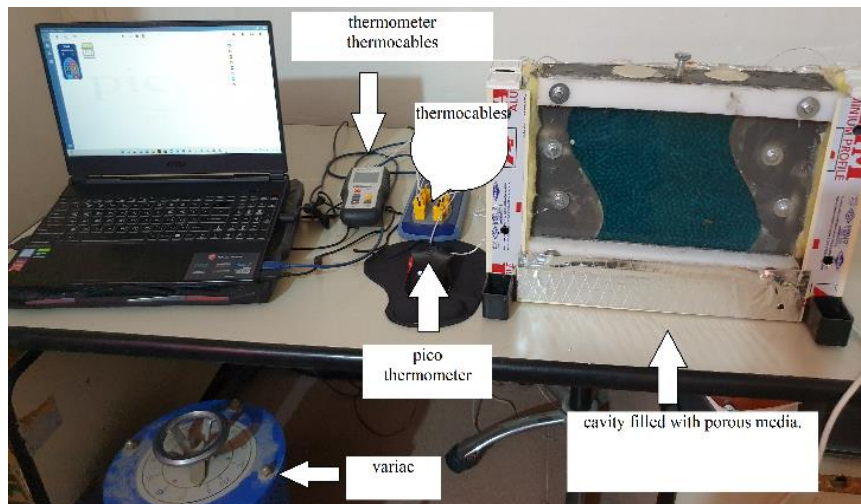


Fig. 1. Test rig (photographically)

### 2.1 Development of the Experimental Model

Three types of wavy cavities (models) with varying height walls were created, produced, and used in the experimental test. These include wavy cavities with wall heights (20, 25, 30 cm). These four elements make up the majority of the proposed mechanism

- i. Designing of the test model
- ii. Electric heater circuit
- iii. Thermocouples
- iv. Measuring equipment

### 2.1.1 Designing of the test model

Three cavities with wave grooves were designed to test the heat transfer properties throughout the porous media and the water. The dimensions selected for the cavity were 20, 25 and 30 cm, in terms of heights, while the width was 20 cm, and the wave groove amplitude was 3cm. For that reason, three aspect ratios (1, 1.25 and 1.5) were examined, respectively.

The cavity was made on Teflon with a wave thickness of 27 mm by using a computer numerical control machine (CNC). Solid material was used it can bear high-temperature values. Six holes (3 for each side) were made along the wall towards the cavity, in a diameter suitable for thermocouples, which was fixed with epoxy (more details can be found in Section 2.3.1). On top of that, the front face was covered with heat-resistant transparent plastic with a thickness of 5 mm, whereas it was fixed over the Teflon sheet with eight bolts by using a dice tool. Then, high-temperature silicon coat being was applied on the sides to avoid any leakage of water. The top and bottom gaps were sealed with an aluminum sheet of 3 mm thickness by using screws and thermal silicon. The top aluminum sheet contained two thermocouples, while the bottom sheet contained three thermocouples and a halogen heat source. Before installing the upper part, the gap was filled with glass beads and alumina saturated with water. The test system was thermally isolated by using sheets of glass wool on three sides (left, right and back sides). Finally, the designed system was fixed with an aluminum frame. The general properties of Teflon, high-temperature plastic, and aluminum are shown in Table 1.

**Table 1**  
General properties of the employed materials

Properties	Teflon	Pyrex	Aluminum
Melting point	327 °C (600 °K)	160 °C (433 K)	660°C(933K)
Thermal conductivity	0.25 W/(m·K)	0.17 – 0.2 W/(m·K)	204 W/(m·K)

#### 2.1.1.1 Steps for producing a cavity

Firstly, an Auto cad program was employed to design the geometry. Secondly, drilling machines with CNC programming were used to create the three different types of test models, as indicated in Figure 2. The sides, back wall, and bottom base of the device were coated with a sheet layer of glass wool that had a thermal conductivity of 0.04 (W/m. k) to improve the complete insulation feature. The glass wool must be present on the sidewalls of the device to decrease the heat losses through the teats section to the environment.

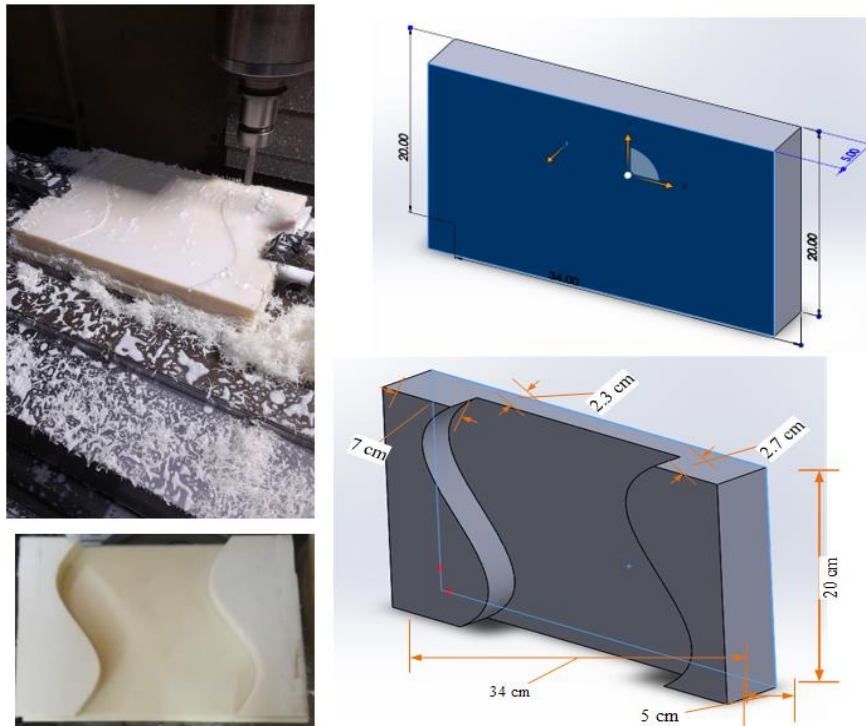


**Fig. 2.** Schematic illustration of the cavity

### 2.1.2 Heater circuit

Figure 3 depicts the heater circuit for the heating element. More specifically, it consists of a Slide Regulator Variac. The variable transformation was also used to change the appropriate heater input power, and a digital AC clamp meter was used to determine the heater voltage and the current. A halogen heater (1000 W/220 V) was placed at the bottom surface of the test cavity to electrically heat it, while an enclosure was placed inside to produce the necessary constant, uniform heat flux. This kind of heater can produce heat by converting a sizable portion of the received energy.

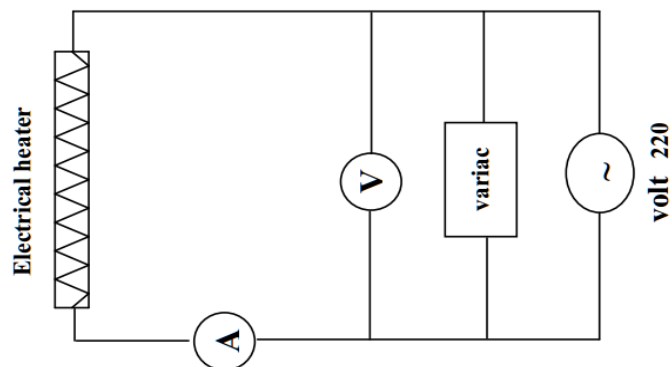


**Fig. 3.** Depiction of the heater's circuit

### 2.1.3 The circuit of thermocouple

In the thermocouple circuit, two electronic digital thermometers of Pico Technology Data Logger and a thermocouple thermometer connected into the thermocouples (type K) were used. It consisted of twelve connection points, characterized by excellent resolution, precision, USB connected and powered. All the employed thermocouples were regulated by Central Organization for

standardization and quality control (COSQC). The calibration is shown in Figure 4, where the relationship between the actual value and the indicated value can be observed.

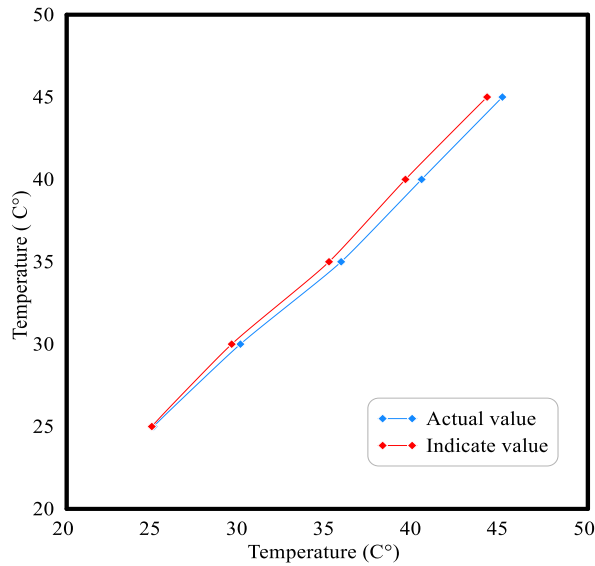


**Fig. 4.** Difference between the actual and the indicated values

#### 2.1.3.1 Arrangement of the thermocouples

By using 11 thermocouples wire (type K) to measure the temperature distribution in an enclosure, which consists of (Chromel 90 % Ni- 10% Cr; Alumel 95%Ni- 2% Al- 3%Mn) arranged uniformly on top, bottom surfaces and on the wavy sidewalls. Because a wide range of temperature values (-270 to 1260 °C) can be measured, they respond quickly, offer good resistance to oxidation, and have time Special Limits of Error of 0.4 percent. This type of thermocouple has been also utilized in a variety of applications. The drilling of the hole included two steps. Firstly, a hole with a diameter of 3 mm was drilled. Secondly, a hole with a diameter of 1 mm was drilled and then the thermocouple was inserted and fixed by using mitreapel adhesive with spray and thermal epoxy, as is shown in Figure 5.



**Fig. 5.** Location of the fixed thermocouples

The depth values of the wall vary according to where the thermocouples were placed, as can be ascertained from Figure 6 and Figure 7.

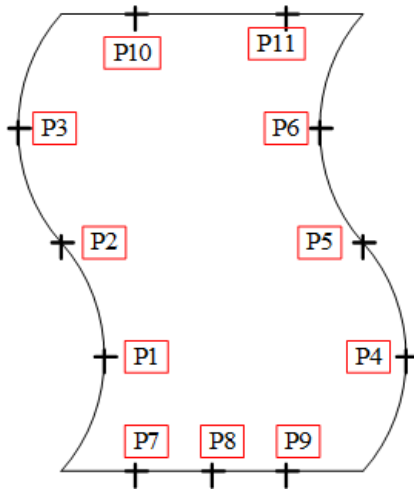


**Fig. 6.** Distribution of the thermocouples

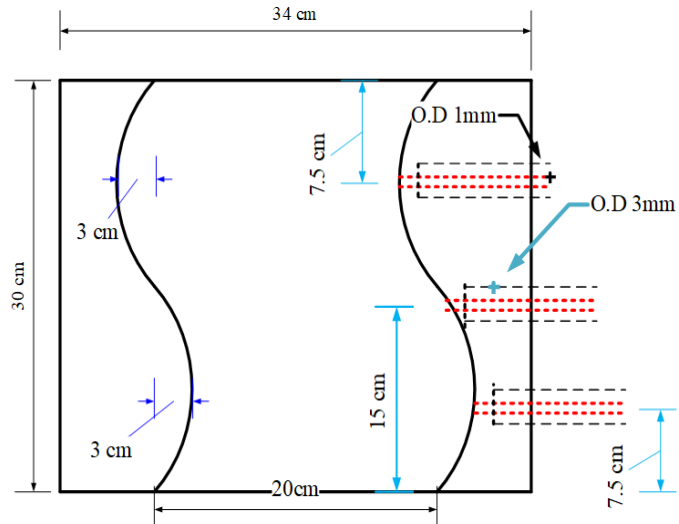


**Fig. 7.** Installation of the thermocouple and its depth in the sidewall

#### 2.1.4 Instrument devices

Due to the various involved limits, the temperature measurements are conducted with electric variables. However, many distinct types of instrument plans were employed in this experimental work.

##### 2.1.4.1 Variable transformer

Figure 8 shows a manual voltage transformer changer (Variac). It possesses gradients for input voltage degree (from 1 to 220 volts), output voltage degree (from 0 to 220 V), capacity (6.6 KVA / 30 A), and frequency (50/60 Hz). Thus, the heater's input power can be adjusted as necessary. In this work, the provided voltage values ranged from 2 to 8 V.



**Fig. 8.** Depiction of a manual voltage changer (Variac)

##### 2.1.4.2 Temperature data logger

Figure 9 displays the Pico Technology Data Logger that was employed to measure the eight thermocouples channel. The readings can be made between (-270 to +1820) C°. It stands out for its

high resolution and accuracy, USB connection, and ability to store an enhanced amount of reading data.



Fig. 9. Image of the Pico data logger

#### 2.1.4.3 Thermocouple thermometer

A digital LCD display with a backlight, easy read process, and Handheld portable design was used for the read-out procedure of the temperature measurements. The thermometer is portable, supports Celsius, Fahrenheit and Kelvin conversion, it possesses four channels for simultaneous measurement and display, and is convenient to use. An image of the employed thermocouple is shown in Figure 10.



Fig. 10. Image of the thermocouple thermometer

#### 2.1.4.4 Clamp meter

Figure 11 depicts a digital AC clamp meter (TMT46002 type, Max. 600 V, 600 A). These meters have the ability to measure current, voltage, resistance, and capacitance. To calculate the amount of power based on the supply voltages and provide the thermal flux, it was utilized to measure the delivered current by the heater in the experimental work.



**Fig. 11.** Image of the clamp meter

#### 2.1.4.5 Digital temperature laser gun

A digital temperature was used to measure the ambient laboratory temperature. It can measure temperature values that range from  $-30\text{ }^{\circ}\text{C}$  to  $500\text{ }^{\circ}\text{C}$ , with a distance coefficient ratio of 10:1, response time less than 500 ms, and emissivity from 0.1 to 1, as is shown in Figure 12.



**Fig. 12.** Image of the digital temperature gun

## 2.2 Porosity Calculation

The term "porosity" refers to the proportion of the cavity's total volume ( $V_{total}$ ) to its pore volume ( $V_{porous}$ ), which varies depending on the packing method. Two methods were used to calculate the porosity in this work. The initial approach, which was based on the implementation of an empirical equation from Salman *et al.*, [12], which can be expressed as follows:

$$\varepsilon = 0.3454 + 11.6985 (Dp) \quad (1)$$

During the experiments, glass balls with diameters (3, 6, 10) mm and alumina balls with a diameter of 6 mm were used, as shown in Figure 13.

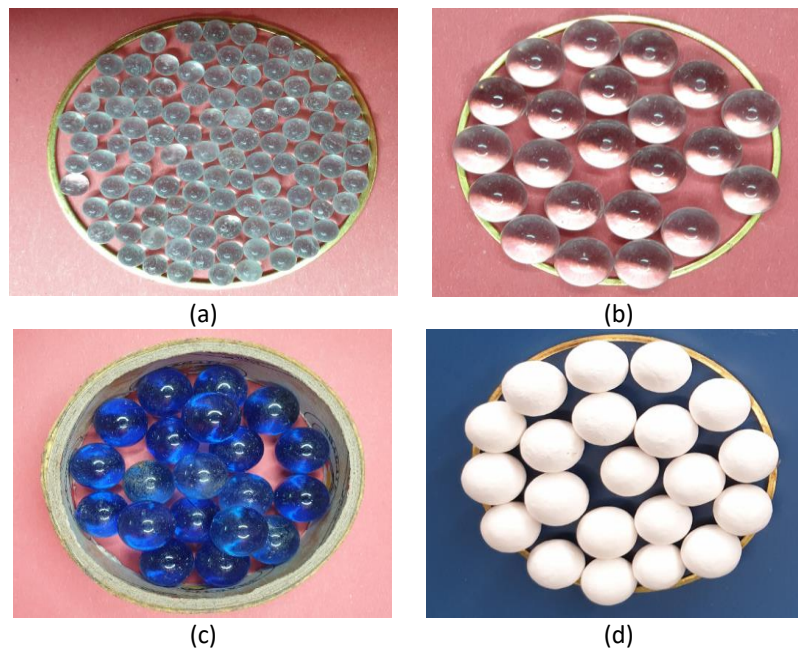


**Fig. 13.** Images of the various porous media beds; (a) Glass 3 mm, (b) Glass 6 mm, (c) Glass 10 mm, (d) Alumina 6 mm

The second method involved the execution of experiments by using 300 ml of 3 mm-diameter glass and 300 ml of water. The glass beaker was then filled with water, When the water was saturated, it can be observed that it leaked into the glass cracks and filled them up. Then, remaining water raised over the saturated glass. To determine the porosity, after subtracting the specified sum from the total volume of the water, the total volume was divided. Table 2 compares the values of porosity that were determined by employing Eq. (1) and their values that have been determined experimentally

$$V_s = V_{total} = 300ml$$

$$V_{wa1} = 300ml$$

For glass porous diameter (3 mm)

$$V_{wa2} = 185ml$$

$$v_{po} = v_{wa1} - v_{wa2} = 300 - 186 = 114ml$$

$$\varepsilon = \frac{v_{po}}{v_{total}} = \frac{114}{300} = 0.38$$

For glass porous diameter (10 mm)

$$v_{wa2} = 160ml$$

$$v_{po} = v_{wa1} - v_{wa2} = 300 - 160 = 140$$

$$\varepsilon = \frac{v_{po}}{v_{total}} = \frac{140}{300} = 0.466$$



**Fig. 14.** Experimental calculation of the porosity for a glass with a diameter of 3 mm



**Fig. 15.** Experimental calculation of the porosity for a glass with a diameter of 10 mm

**Table 2**

Porosity from Eq. (1) and compared with the experimental results

Porous diameter	Particle test	From Eq. (1)
3 mm	0.38	0.38
6 mm	0.417	0.415
10 mm	0.466	0.462

### 2.3 Permeability

The number that represents the rate of the fluid flow through a porous medium is known as permeability (K). It is regarded as a crucial quality of the porous bead. The unit scales for permeability are Darcy (D) or square lengths ( $L^2$ ). In this work, the permeability was calculated in two different ways: theoretically by using geometrical parameters from Sadeq [13], such as the diameter of the

porous material and its porosity as described in Eq. (2) and experimentally by using Darcy's law. Table 3 displays the permeability values for the various diameters of the porous materials that were used.

$$K = \frac{\epsilon^3 \times Dp}{150 \times (1-\epsilon)^2} \quad (2)$$

**Table 3**  
 The permeability of the porous materials

Porous diameter	Permeability
3 mm	$8.56483 \times 10^{-9} \text{ m}^2$
6 mm	$5.01238 \times 10^{-8} \text{ m}^2$
10 mm	$2.27127 \times 10^{-7} \text{ m}^2$

## 2.4 Experimental Work Setup

Each of the three types of cavities were considered separately, whereas their components and thermal conductors were installed, so that only the head of the conductor was visible to sense heat. In addition, these conductors were connected to devices that can read the transmitted temperature in 11 locations, three on each side, three at the base, and two above the metal recess. This information was used to calculate the amount of the transferred heat in porous materials by natural convection inside each of the three types of cavities.

- i. The cavity was completely filled with glass, making sure that there is no vacuum inside the cavity. The glass was then gradually filled with water until it was fully saturated, and the cavity was then sealed off with a metal piece and fastened with screws and thermal silicone to ensure that any heat leakage outside is prevented.
- ii. The voltage and current requirements were ascertained to ensure the existence of the necessary heat power before starting.
- iii. A limited voltage was provided to flow the current via the heat source (a halogen heater), generating the necessary power to provide the desired quantity of constant heat flux (300, 500, 700, 900, 1100)  $\text{W/m}^2$  that was imposed on the bottom surface of the cavity.
- iv. Prior to the commencement of the operation, various environmental conditions including the room temperature were detected by a laser temperature gun and noted, along with the temperature value of all cavities.
- v. After the procedure, the initial temperature reading was taken after about 30 minutes. Thereafter, the readings were taken every 10 minutes for a while, then every 5 minutes, until a steady state was attained, which was reached after about 3.5 to 4 hours.
- vi. To determine the best heat transfer process, this procedure was repeated for five different voltages (2.75, 4.16, 5.18, 6.4, and 7.16) V, which were applied in three types of cavities: glass with three diameters of 3 mm, 6 mm, and 10 mm, and alumina with a diameter of 6 mm.



**Fig. 16.** Depiction of the three cavities filled with porous

### 3. Calculations of Parameters

To calculate the amount of heat transferred and other parameters from the practically recorded temperatures, they are listed as follows

- i. Power supply to the heater can be calculated as following [14]

$$Q = V \times I \times \cos \theta \quad (3)$$

where, Q: Electrical power consumed by the heater in Watt,  $\theta$ : Phase shift angle (power factor) for three phases. Note: -  $\cos(\theta) = 1$  for heater.

- ii. Heat flux equal to heat input the system [15]

$$\bar{q} = \frac{Q}{A} \quad (4)$$

A = width x depth of cavity = W x Z

- iii. The heat losses from cavity to the ambient with the side wall, front and back wall.

$q_{fr}$  = The front wall heat losses (W/m<sup>2</sup>).

$q_{ba}$  = The back wall heat losses (W/m<sup>2</sup>)

$q_{si}$  = The sides wall heat losses (W/m<sup>2</sup>).

$$q_{losses} = q_{fr} + q_{ba} + q_{si} = \text{Total heat losses} \quad (5)$$

$$q_{in} = q_{out} - q_{losses} \quad (6)$$

After determinations of the net heat flux, this step explains the calculation of other parameters [16]

$\Delta T$ : is the difference between the average base temperature and average bulk temperature where

$T_{bulk}$ : is the average temperature of the cavity except the temperature base of the cavity.

$T_{base}$ : is the average temperature of base cavity.

$$\Delta T = T_{base} - T_{bulk}$$

$$T_f = \frac{T_{base} + T_{bulk}}{2}$$

$$h = \frac{\bar{q}_{net}}{\Delta T}$$

$$K_{eff} = \varepsilon \times k_f + (1 - \varepsilon) \times k_{solid} \quad (7)$$

$$H = \frac{4A_c}{p} \quad (8)$$

$$Nue = \frac{h*H}{K_{eff}} \quad (9)$$

$$Gr_r = \frac{g*\beta*\Delta T*d^3}{\nu^2} = Gr_r \times p_r \quad (10)$$

$$Ra_m = (Gr \times Pr) \times Da \quad (11)$$

$$Da = \frac{K}{H^2} \quad (12)$$

#### 4. Results and Discussion

##### 4.1 Impact of Aspect Ratio on the Temperature Distribution

As can be observed from Figure 17 to Figure 20, the influence of the aspect ratio on the temperature difference is illustrated, the highest temperature difference between the top of the cavity and the bottom was obtained when  $As = 1$ . The origins of this effect are associated with the fact that the distance needed by the fluid to move from the bottom of the enclosure to the upper surface was smaller, and thus, the highest temperature difference was obtained when  $As = 1$ . The increase in the aspect ratio led also to a decrease in  $\Delta T$ .

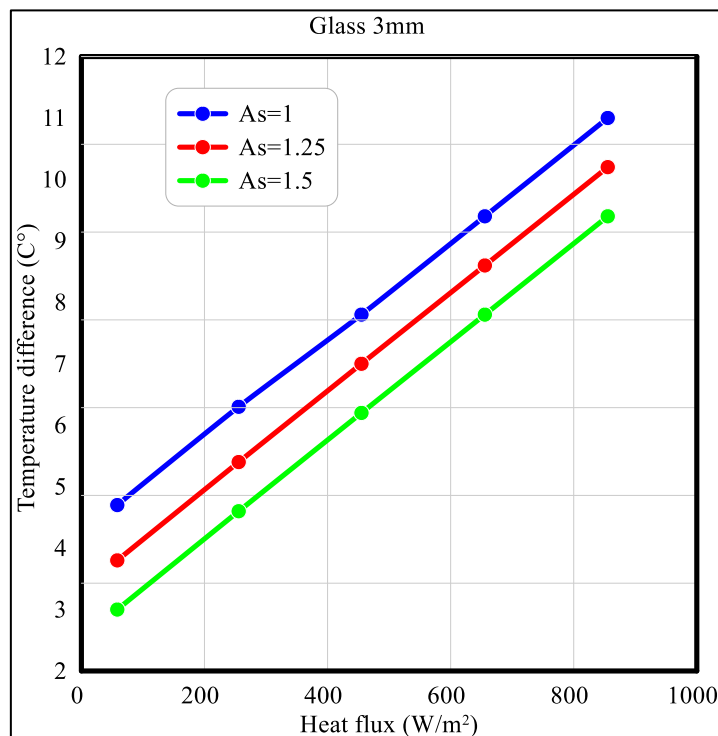


**Fig. 17.** Temperature distribution of glass with a diameter of 3 mm and different aspect ratios

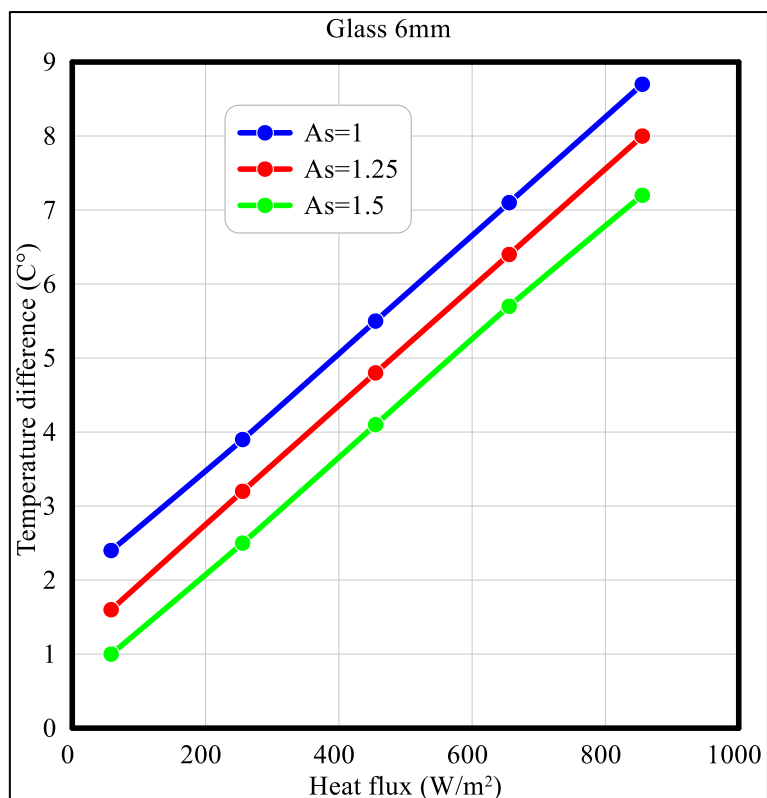


**Fig. 18.** Temperature distribution of glass with a diameter of 6 mm and different aspect ratios

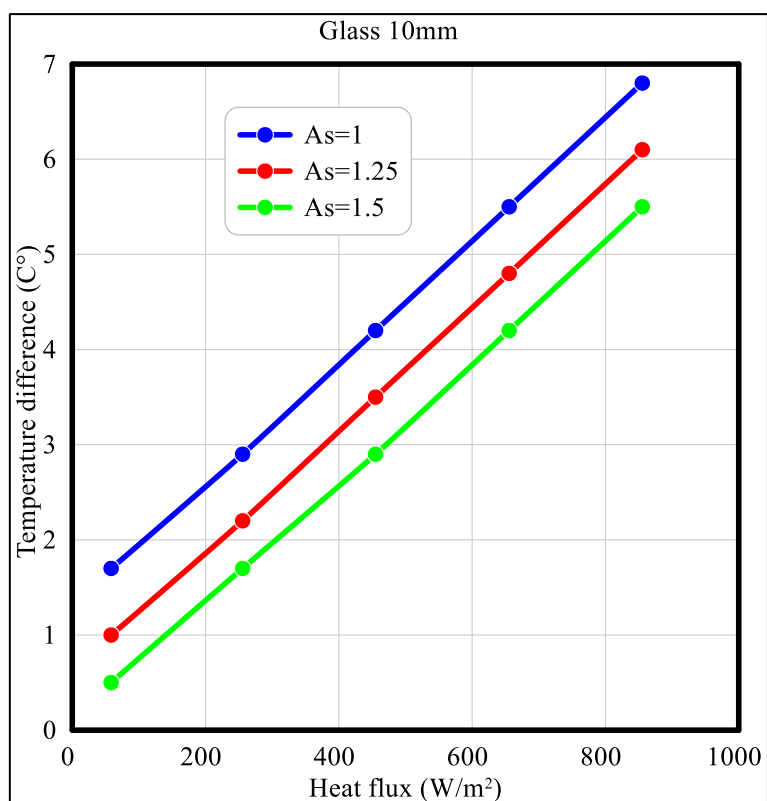


**Fig. 19.** Temperature distribution of glass with a diameter of 10 mm and different aspect ratios

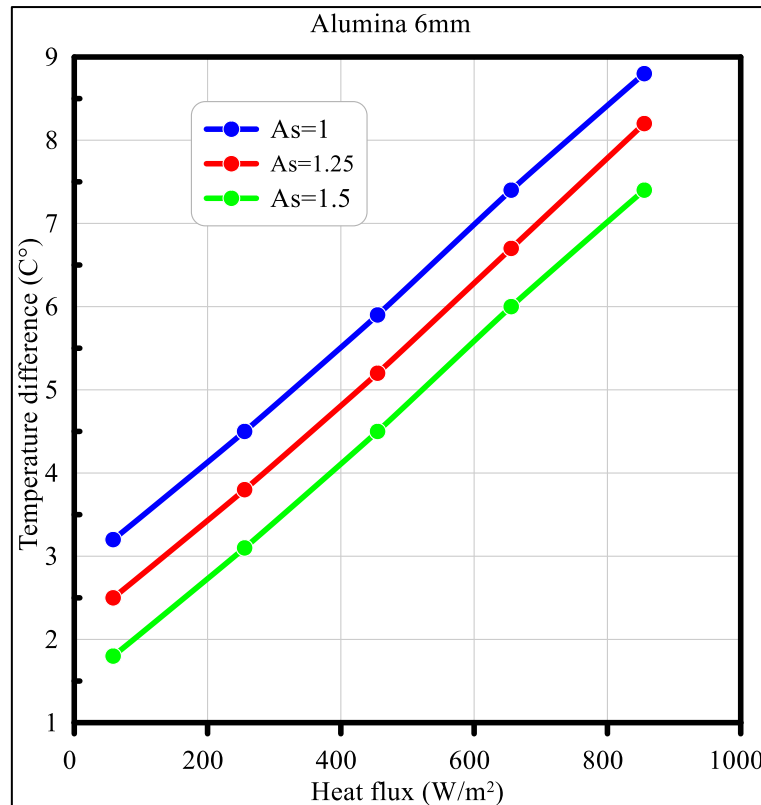


**Fig. 20.** Temperature distribution of Alumina with a diameter of 6mm and different aspect ratios

#### 4.2 Impact of the Temperature Distribution and the Diameter of the Porous Materials

From Figure 21 to Figure 23 explain the relationship between the amount of thermal flux and the temperature difference, which has been studied depending on the difference in diameter and utilizing glass and alumina as a saturated porous media for the three different types of cavities. As can be ascertained from the extracted data, generally speaking, for each diameter of 3 mm, 6 mm, and 10 mm for the glass material and 6 mm for alumina, the amount of the temperature difference is increased with the increase in the thermal flux. For all levels of the thermal flux and all the different models that have been examined, the temperature difference is enhanced as the diameter is decreased, while the measured value at 3 mm was substantially larger than the respective value at 6 mm and 10 mm. This effect can be attributed to the fact that an increase in the thermal flux causes the faster expansion of the thermal layer, which raises the buoyancy strength of all models.

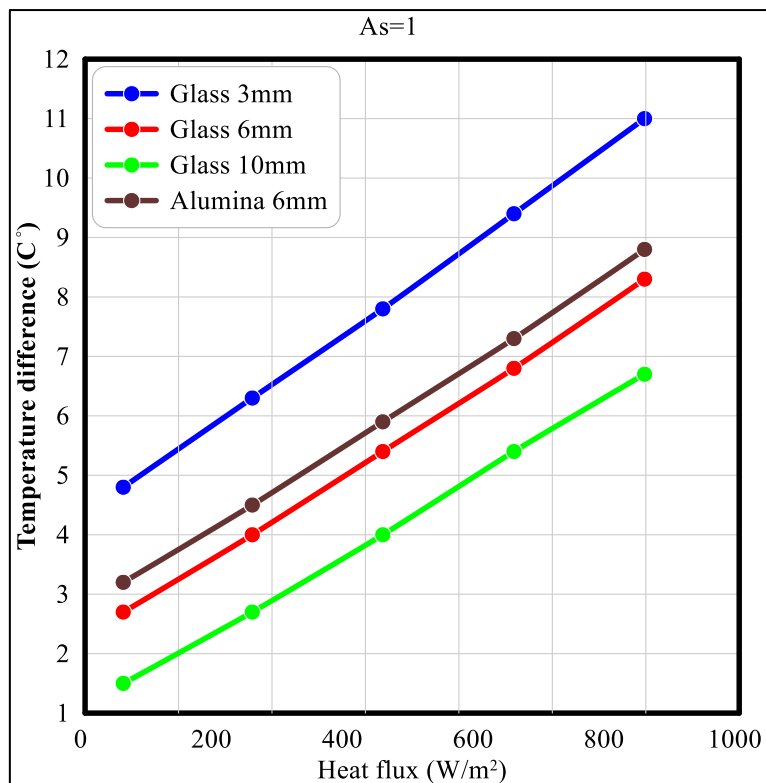


Fig. 21. Distribution of temperature in various porous materials when  $As=1$  was used

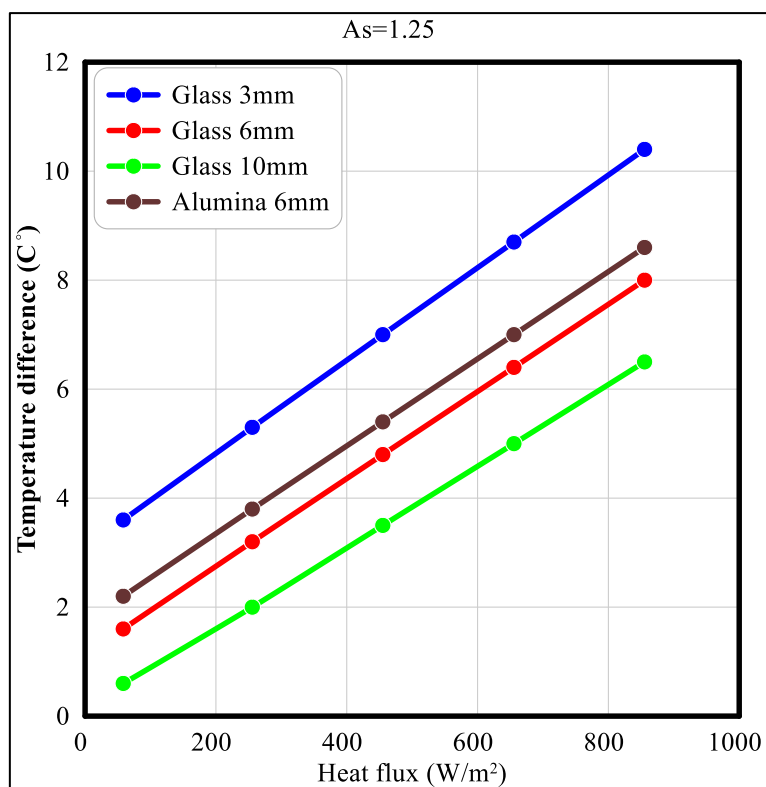
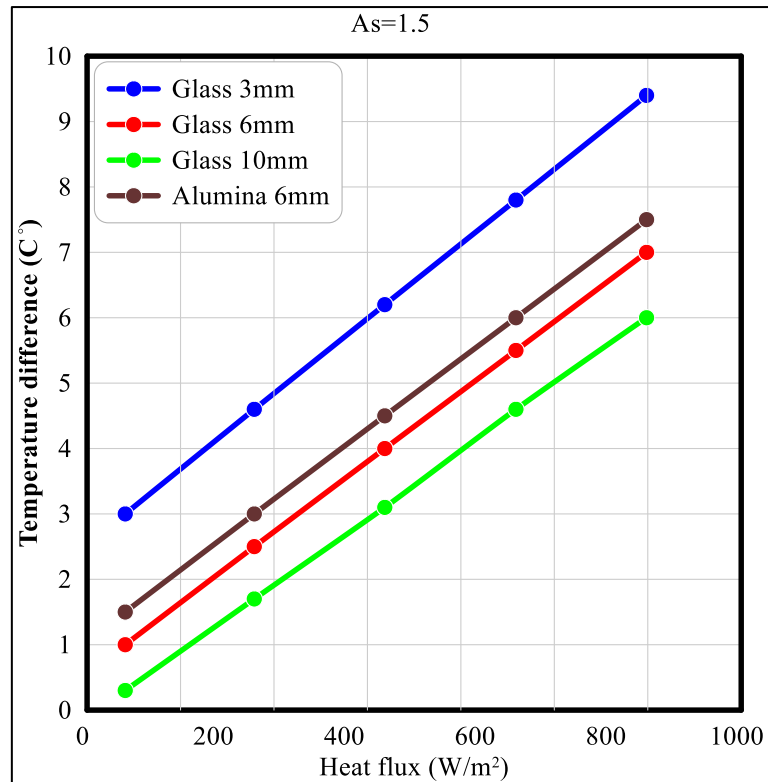


Fig. 22. Distribution of temperature in various porous materials when  $As=1.25$  was used



**Fig. 23.** Distribution of temperature in various porous materials when  $As=1.5$  was used

#### 4.3 Influence of the Aspect Ratio on $Ra_m$

The influence of the aspect ratio on the modified Rayleigh number for different heat fluxes, which was studied experimentally, is shown in Figure 24 to Figure 27. By comparing the different aspect ratios ( $As = 1, 1.25, 1.5$ ), the highest value for modified Rayleigh was obtained when  $As = 1$  because the increase in the aspect ratio led to a decrease in the contact area, which in turn caused a drop in the temperature difference between the base and the bulk. The value of  $Ra_m$  increased as the porous diameter became bigger. An enhanced porous diameter leads to an increase in the porosity, which in turn could increase the permeability and thus, lead to bigger values for the Darcy number.

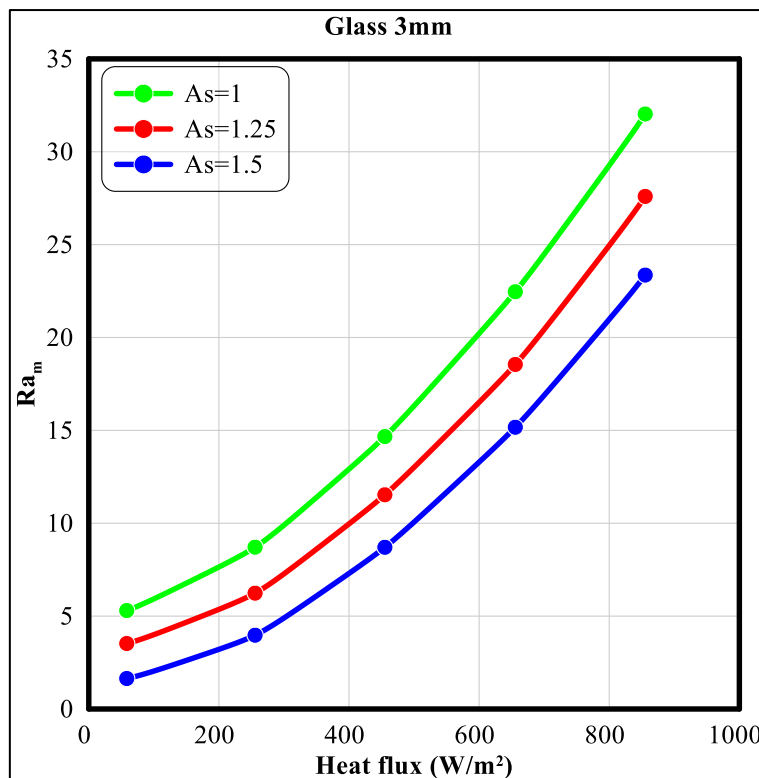


Fig. 24. Distribution of  $Ra_m$  against heat flux for glass porous with a diameter of 3 mm and different aspect ratios

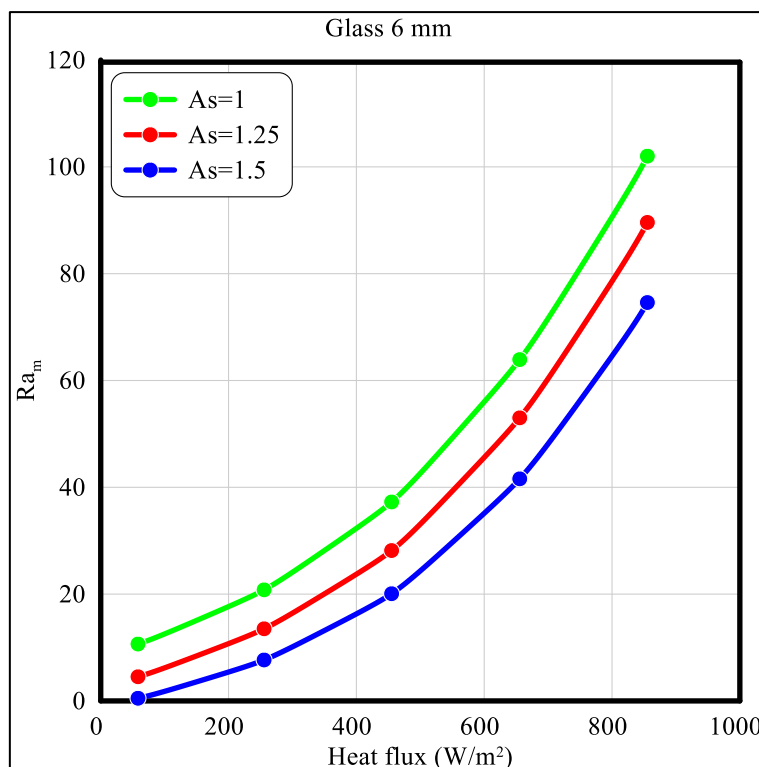
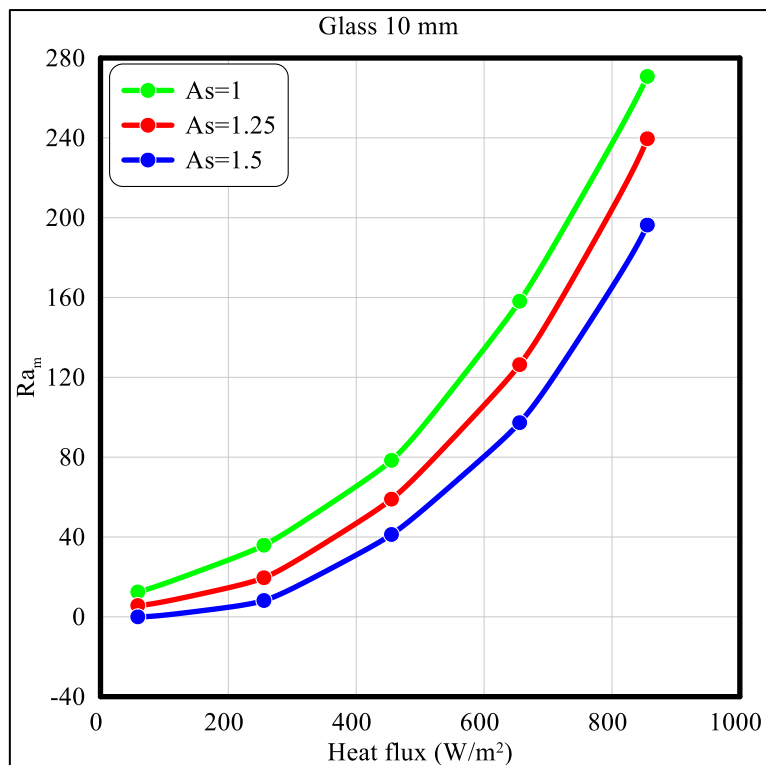
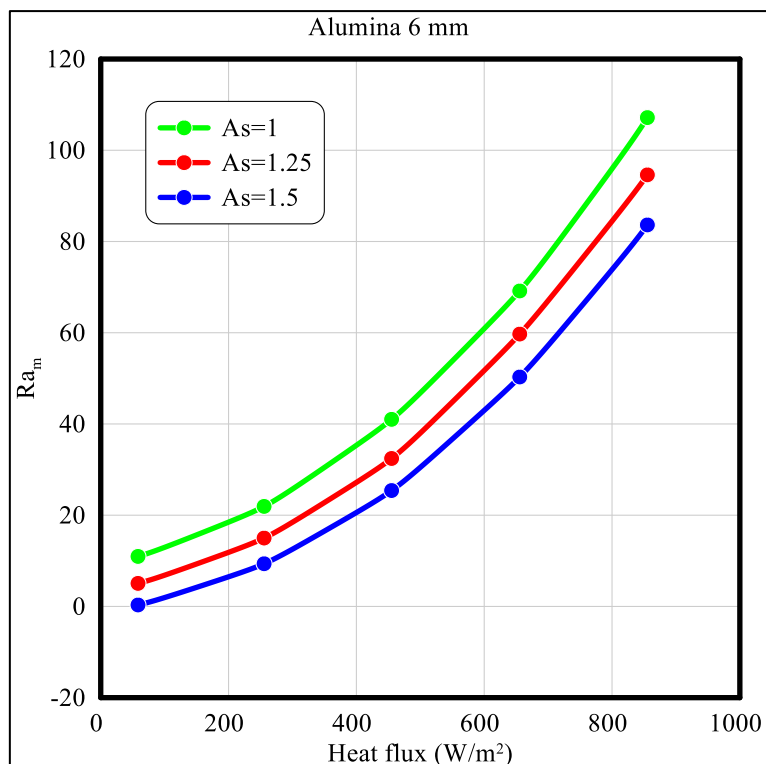


Fig. 25. Distribution of  $Ra_m$  against heat flux for glass porous with a diameter of 6 mm and different aspect ratios



**Fig. 26.** Distribution of  $Ra_m$  against heat flux for glass porous with a diameter of 10 mm and different aspect ratios



**Fig. 27.** Distribution of  $Ra_m$  against heat flux for alumina with a diameter of 6 mm and different aspect ratios

## 5. Conclusions

In this work, a thorough experimental investigation of a corrugated porous cavity was performed, while from the impact of aspect ratio on the natural convection exposed to a continuous heat flow from the bottom surface the following conclusions can be drawn.

The heat transfer coefficient decreases with the increase in the length to the width ratio of the container. Highest value is when aspect ratio is 1. Aspect ratio 1.5 gives the highest value for the Nusselt number. This is because the height of the Nusselt number is directly proportional to the temperature difference, which results in the lowest heat transfer coefficient values. The diameter of the porous material affects the Nusselt number. The diameter of the glass 10 mm gives the highest values of the Nusselt number relative to the diameter 3 and 6 mm by 10% and 20% percent, respectively. The improved Rayleigh number decreases as the aspect ratio increases by 10%. It turned out that the porous material made of alumina gave the maximum heat transfer relative to glass, because it has a higher heat capacity than glass. It also became apparent that the improved Rayleigh number for all models used increased with increased heat flux applied to the base of the container.

## Acknowledgement

I would like to express my deep thanks to my supervisor Prof. Dr. Zena Khalefa Kadhim, I am very grateful for her guidance, advice, invaluable discussions and constructive comment, which greatly improved the structure and presentation of this paper ("This research was not funded by any grant").

## References

- [1] Nield, Donald A., and Adrian Bejan. *Convection in Porous Media*. 4<sup>th</sup> ed. Springer, 2013.
- [2] Cheong, H. T., Zailan Siri, and S. Sivasankaran. "Effect of aspect ratio on natural convection in an inclined rectangular enclosure with sinusoidal boundary condition." *International Communications in Heat and Mass Transfer* 45 (2013): 75-85. <https://doi.org/10.1016/j.icheatmasstransfer.2013.04.017>
- [3] Gati'a, Ali Maseer, Zena Khalifa Kadhim, and Ahmad Kadhim Al-Shara. "Experimental Study of Free Convection Inside Curvy Surfaces Porous Cavity." *Engineering Science* 2, no. 4 (2017): 85-92.
- [4] Mehryan, Seyed A. M., Farshad M. Kashkooli, Mohammad Ghalambaz, and Ali J. Chamkha. "Free convection of hybrid Al<sub>2</sub>O<sub>3</sub>-Cu water nanofluid in a differentially heated porous cavity." *Advanced Powder Technology* 28, no. 9 (2017): 2295-2305. <https://doi.org/10.1016/j.appt.2017.06.011>
- [5] Ali, I. R., Ammar I. Alsabery, Norhaliza Abu Bakar, and Rozaini Roslan. "Mixed Convection in a Lid-Driven Horizontal Rectangular Cavity Filled with Hybrid Nanofluid by Finite Volume Method." *Journal of Advanced Research in Fluid Mechanics and Thermal Sciences* 93, no. 1 (2022): 110-122. <https://doi.org/10.37934/arfmts.93.1.110122>
- [6] Ferhi, Mokhtar, Ridha Djebali, and Said Abboudi. "Conjugate Natural Convection in a Partitioned Square Cavity Filled with Al<sub>2</sub>O<sub>3</sub>-Water Nanofluid Based on Experimental Correlations: a Lattice Boltzmann investigation." *CFD Letters* 11, no. 3 (2019): 1-27.
- [7] Mahdavi, Mahboobe, Saeed Tiari, Ali Heidari, and Majid Saffar Avval. "Experimental and numerical study of heat transfer enhancement in a pipe partially or totally filled with a porous material." In *Proceedings of 3rd Thermal and Fluids Engineering Summer Conference*, pp. 1547-1551. Begel House Inc., 2018. <https://doi.org/10.1615/TFEC2018.prm.022071>
- [8] Cimpean, D. S., C. Revnic, and I. Pop. "Natural convection in a square inclined cavity filled with a porous medium with sinusoidal temperature distribution on both side walls." *Transport in Porous Media* 130, no. 2 (2019): 391-404. <https://doi.org/10.1007/s11242-019-01315-w>
- [9] Bakar, Norhaliza Abu, Rozaini Roslan, and Mohd Kamalrulzaman Md Akhir. "The Effects of Internal Heat Generation or Absorption on Mixed Convection in a Lid-Driven Rectangular Cavity using Finite Volume Method." *CFD Letters* 12, no. 12 (2020): 38-54. <https://doi.org/10.37934/cfdl.12.12.3854>
- [10] Barman, Prabir, and P. S. Rao. "Effect of aspect ratio on natural convection in a wavy porous cavity submitted to a partial heat source." *International Communications in Heat and Mass Transfer* 126 (2021): 105453. <https://doi.org/10.1016/j.icheatmasstransfer.2021.105453>

- [11] Al-Farhany, Khaled, and Ahmed Dhafer Abdulsahib. "Study of mixed convection in two layers of saturated porous medium and nanofluid with rotating circular cylinder." *Progress in Nuclear Energy* 135 (2021): 103723. <https://doi.org/10.1016/j.pnucene.2021.103723>
- [12] Salman, Abdul Hakeem A., Kifah H. Hilal, and Safaa A. Ghadhban. "Enhancing performance of PV module using water flow through porous media." *Case Studies in Thermal Engineering* 34 (2022): 102000. <https://doi.org/10.1016/j.csite.2022.102000>
- [13] Sadeq, Mays Subhi. "Experimental and Numerical Study of Natural convection inside sinusoidal surface cavity filled with various porous media." *Master thesis, College of Engineering, Wasit University, 2020.*
- [14] Mahmood, Abeer Aamer. "Study of the free and forced convection heat transfer around a cylinder embedded in porous media." *Master thesis, Mechanical Engineering Department, University of Technology, Iraq, 2016.*
- [15] Holman, J. P. *Experimental Methods for Engineers*. 18<sup>th</sup> ed. McGraw Hill, 2012.
- [16] Holman, J. P. *Heat Transfer*. 10<sup>th</sup> ed. McGraw Hill, 2010.
- [17] Hilal, Kifah Hamed. "Fluid Flow and heat transfer characteristics in a tube packed bed media." *PhD diss., Mechanical Engineering Department, University of Technology, Iraq, 2004.*